A semi-empirical method for the estimation of the hydration number of Mn(II)-complexes

Peters, Joop A.; Geraldes, Carlos F.G.C.

Important note
To cite this publication, please use the final published version (if applicable).
Please check the document version above.

A Semi-Empirical Method for the Estimation of the Hydration Number of Mn(II)-Complexes

Joop A. Peters [1],* and Carlos F. G. C. Geraldes [2],*

[1]   Laboratory of Biocatalysis, Delft University of Technology, Van der Maasweg 9,
     2629 HZ Delft, The Netherlands
[2]   Department of Life Sciences and Coimbra Chemistry Centre, Faculty of Science and Technology,
     University of Coimbra, Calçada Martim de Freitas, 3000-456 Coimbra, Portugal
*   Correspondence: j.a.peters@tudelft.nl (J.A.P.); geraldes@ci.uc.pt (C.F.G.C.G.);
     Tel.: +351-239-240-730 (C.F.G.C.G.)

check for updates

Abstract: A semi-empirical equation to estimate the hydration number of Mn(II) complexes was derived from a database of 49 previously published ^{1}H longitudinal Nuclear Magnetic Relaxation Dispersion profiles. This equation has the longitudinal ^{1}H relaxivity and the molecular weight of the Mn(II) complex under consideration as parameters.

1. Introduction

During the last decades, Gd^{3+}-chelates, such as Gd-DTPA (DTPA = diethylenetriamine-*N*,*N*,*N'*,*N''*,*N''*,*N'''*-pentaacetate) and Gd-DOTA (DOTA = 1,4,7,10-tetraazacyclododecane-*N*,*N'*,*N''*,*N'''*-tetraacetate), have become indispensable tools for the contrast enhancement of magnetic resonance images [1–3]. These contrast agents (CAs) have proven to be generally extremely safe; only 0.03% of all administrations (about 100 million worldwide) gave rise to serious adverse effects. However, during recent years, some concerns have arisen because of (i) incidents of nephrogenic systemic fibrosis (NSF) associated with Gd^{3+}-complexes of linear DTPA derivates and (ii) observation of Gd-accumulation in the brains of patients with normal renal function, after repeated administrations of DTPA-type of CAs [4–8]. Both effects may be ascribed to the relative kinetic instability of Gd^{3+} complexes of linear polyaminocarboxylates. The concerns about Gd-based CAs have led to an increased interest in application of Gd^{3+}-free CAs. High spin d^5 Mn^{2+} is an attractive alternative for f^7 Gd^{3+}, because it has only two less unpaired electrons, whereas a high electronic symmetry is favorable for high relaxivities. Moreover, Mn^{2+} is less toxic than Gd^{3+}, as reflected in its important role as a cofactor in many enzymatic reactions, including the anti-oxidant enzyme superoxide dismutase, as well as in enzymes involved in neurotransmitter synthesis and metabolism in the brain. However, the concentration of free Mn^{2+} in organisms is very low, for instance 0.3–1 µg·L^{-1} in human blood [9]. High concentrations are neurotoxic, and therefore, Mn^{2+} preferably needs to be sequestered for safe application as CA in humans. Due to its lower charge, complexes are usually less stable than their Gd^{3+}-counterparts. It is important to assure that the dissociation of Mn^{2+}-based CAs is minimized in order to avoid any neurotoxic side effects. On the other hand, the relaxation rate enhancing efficacy should be as high as possible in view of the inherently low sensitivity of magnetic resonance imaging (MRI) CAs. Finding a balance between kinetic stability and optimal sensitivity is a challenge during the design of novel Mn^{2+}-based CAs.

The efficacy of a CA is usually expressed by its relaxivity, the longitudinal, or transverse relaxation rate enhancement normalized for a solution containing 1 mM of paramagnetic metal ions (r_1 and

r_2, respectively). One of the most important parameters governing the longitudinal relaxivity (r_1) of paramagnetic CAs is the number of water molecules in the first coordination sphere of the metal ion (q), since the inner sphere contribution to r_1 is linearly proportional to it. Several good methods are available to evaluate q for Gd^{3+}-based CAs, including measurements of lanthanide induced ^{17}O NMR shifts (NMR = Nuclear Magnetic Resonance) of water [1,10,11], determination of the ^{17}O scalar coupling constant ($A_O/\hbar$) from simultaneous fitting of ^{17}O shift and/or relaxation data and ^1H NMRD data (NMRD = Nuclear Magnetic Relaxation Dispersion), and comparison of the luminescence decay rates of Eu^{3+} or Tb^{3+} complexes in H_2O and D_2O [12]. The determination of q for Mn^{2+}-complexes is more challenging. The luminescence decay method is impossible, because the complexes are not luminescent. ^{17}O NMR methods are more ambiguous since they rely on the assumption that $A_O/\hbar$ is almost independent on the coordination environment of Mn^{2+}, which appears not to be case: values in the range $-(26$–$73) \times 10^6$ rad·s^{-1} have been evaluated from ^{17}O NMR measurements on Mn^{2+} complexes (see below, Table 1). Esteban-Gómez et al. have estimated by DFT calculations that variations of Mn–O distances and dihedral angles among these complexes may lead to $A_O/\hbar$ values ranging between 30 and 58×10^6 rad·s^{-1} [13]. By contrast, the range of $A_O/\hbar$ values observed for Gd^{3+}-complexes observed is narrower ($-(3.6$–$4.2) \times 10^6$ rad·s^{-1}) [11], allowing reasonable accurate estimations of q using a ^{17}O NMR shift and/or relaxation rates. Moreover, accurate Mn^{2+}-induced shift measurements are difficult because of the very large line broadenings and relatively small induced shifts.

X-ray crystallography may provide structures of Mn^{2+} complexes in the solid state, but these structures are not necessarily the same in solution. Frequently dimeric or oligomeric assemblies occur in crystal structures, which will dissociate upon dissolution in water. Often, a value of q is estimated based on the denticity of the organic ligand and assuming a total Mn^{2+}-coordination number of 6. However, high spin Mn^{2+}-complexes have almost no ligand stabilization energy, and consequently, do not show a clear preference for a specific coordination number. Others use the magnitudes of the longitudinal relaxivities to estimate q, which is ambiguous as well, as will be demonstrated below. Recently, Póta et al. suggested that DFT calculations (at the M062X/TZVP level) may provide reliable q-values [14]; however, these calculations require excessive amounts of computing time with supercomputers.

Here, we will demonstrate that reliable q values for Mn^{2+}-complexes can be obtained from experimental r_1 values at low Larmor frequencies (*LF*) and the formula weight (*FW*) of the complexes.

2. Results and Discussion

A database of 49 previously published ^1H longitudinal Nuclear Magnetic Relaxation Dispersion profiles (plots of r_1 versus *LF*) was constructed (see Table 1 and Figure 1). The relaxivity has an inner-sphere contribution by water molecules exchanging between the first coordination sphere of the metal ion and the bulk ($r_{i,IS}$) and an outer-sphere contribution due to water molecules in the bulk that diffuse in the surroundings of the metal ion without being bound to it ($r_{1,OS}$) (see Equation (1)). The amount of a Mn^{2+}-based CA needed is always very small (in the mM range) and the Mn^{2+}-induced chemical shifts of the water protons are negligible. Under those conditions, $r_{1,IS}$ was related to the longitudinal relaxation time of a Mn^{2+}-bound water molecule (T_{1M}), according to Equation (2) [15,16]:

$$r_1 = r_{1,IS} + r_{1,OS} \tag{1}$$

$$r_{1,IS} = \frac{q}{55556(T_{1M} + \tau_M)} \tag{2}$$

Here, τ_M is the residence time of a water molecule in the first coordination sphere of Mn^{2+}. Since the electronic relaxation time (T_{1e}) for Mn^{2+}-complexes was generally larger than the rotational correlation time (τ_R), the contribution of the Curie relaxation mechanism to the longitudinal relaxation was negligible; only the dipolar and the scalar mechanisms needed to be taken into

consideration. These contributions ($T_{1M,DD}{}^{-1}$ and $T_{1M,SC}{}^{-1}$, respectively) may be estimated by using the Solomon-Bloembergen-Morgan (SBM) equations (Equations (3)–(7)) [17,18]:

$$\frac{1}{T_{1M}} = \frac{1}{T_{1M,DD}} + \frac{1}{T_{1M,SC}} \tag{3}$$

$$\frac{1}{T_{1,DD}} = \frac{2}{15}\left(\frac{\mu_0}{4\pi}\right)^2 \frac{\hbar^2 \gamma_S^2 \gamma_I^2}{r_{MnH}^6} S(S+1)\left(\frac{3\tau_{d1}}{1+\omega_I^2\tau_{d1}^2} + \frac{7\tau_{d2}}{1+\omega_S^2\tau_{d2}^2}\right) \tag{4}$$

$$\frac{1}{T_{1,SC}} = \frac{S(S+1)}{3}\left(\frac{A_H}{h}\right)^2\left(\frac{2\tau_{s2}}{1+\omega_s^2\tau_{s2}^2}\right) \tag{5}$$

Here, $(\mu_0/4\pi)$ is the magnetic permeability in vacuum, r_{MnH} is the distance between Mn^{2+} and the H-atom of a bound water molecule, S is the electron spin ($S = 5/2$ for Mn^{2+}), γ_I is the ^{1}H nuclear gyromagnetic ratio, γ_S is the electron gyromagnetic ratio, and ω_I and ω_S are the Larmor frequencies of the proton and electron spin, respectively, $A_H/\hbar$ is the hyperfine coupling constant between Mn^{2+} and the bound water proton, $\tau_{di}{}^{-1} = \tau_M{}^{-1} + \tau_R{}^{-1} + T_{ie}{}^{-1}$, and $\tau_{s2}{}^{-1} = \tau_M{}^{-1} + T_{2e}{}^{-1}$. The electronic relaxation times are often interpreted in terms of the zero-field splitting (ZFS) interaction using Equations (6) and (7) [19]:

$$\frac{1}{T_{1e}} = \frac{1}{25}\Delta^2\tau_v[4S(S+1)-3]\left(\frac{1}{1+\omega_s^2\tau_v^2} + \frac{4}{1+4\omega_s^2\tau_v^2}\right) \tag{6}$$

$$\frac{1}{T_{2e}} = \frac{1}{50}\Delta^2\tau_v[4S(S+1)-3]\left(\frac{5}{1+\omega_s^2\tau_v^2} + \frac{2}{1+4\omega_s^2\tau_v^2} + 3\right) \tag{7}$$

In these equations, Δ^2 represents the mean-squared fluctuation of the ZFS, and τ_v is the correlation time for the instantaneous distortion of the coordination polyhedron of Mn^{2+}. From these equations, it can be derived that the low field limiting value of the longitudinal and transverse electronic relaxation rates ($\tau_{S0}{}^{-1}$) were equal, given by Equation (8):

$$\frac{1}{\tau_{S0}} = \frac{1}{5}\Delta^2\tau_v[4S(S+1)-3] \tag{8}$$

The outer-sphere contribution to the relaxivity ($r_{1,OS}$) is described by Equations (9) and (10) [20]:

$$r_{1,OS} = \left(\frac{32\pi}{405}\right)\left(\frac{\mu_0}{4\pi}\right)^2 \gamma_I^2\gamma_S^2\hbar^2 S(S+1)\frac{N_A}{a_{MnH}D_{MnH}}[3J_{OS}(\omega_I, T_{1e}) + 7J_{OS}(\omega_S, T_{2e})] \tag{9}$$

$$J_{OS}(\omega, T_{je}) = Re\left\{\frac{1+\frac{1}{4}\left[i\omega\tau_{MnH}+\left(\frac{\tau_{MnH}}{T_{je}}\right)\right]^{\frac{1}{2}}}{1+\left[i\omega\tau_{MnH}+\left(\frac{\tau_{MnH}}{T_{je}}\right)\right]^{\frac{1}{2}}+\frac{4}{9}\left[i\omega\tau_{MnH}+\left(\frac{\tau_{MNH}}{T_{je}}\right)\right]+\frac{1}{9}\left[i\omega\tau_{MnH}+\left(\frac{\tau_{MnH}}{T_{je}}\right)\right]^{\frac{3}{2}}}\right\} \tag{10}$$

Here, N_A is Avogadro's number, a_{MnH} is the distance of closest approach of a diffusing water molecule to Mn^{2+}, D_{MnH} stands for the diffusion coefficient, and $J_{os}(\omega, T_{je})$ (j = 1, 2) are spin density functions. The diffusion correlation time (τ_{MnH}) is given by $a_{MnH}{}^2/D_{MnH}$.

An inspection of Equations (4) and (5) indicates that in an NMRD profile, two inflection points may be expected: one originating from $1/T_{1,DD}$ when $\omega\tau_{d2} = 1$ (at $LF \approx 10$ MHz), and another one due to $1/T_{1,SC}$ when $\omega\tau_{s2} = 1$ (at $LF \approx 0.06$ MHz) [21,22]. Until now, only two Mn^{II}-based CAs have been observed that have NMRD profiles showing these two inflection points: $[Mn^{II}(H_2O)_6]^{2+}$ [21,22] and $[Mn^{II}_2(ENOTA)(H_2O)_2]$ [23]. All other reported NMRD profiles display only the high field dispersion at $LF \approx 10$ MHz, indicating that for these compounds the contribution of the scalar interaction to the relaxivity is negligible.

It should be noted that the SBM equations, particularly Equations (6) and (7), only hold under certain conditions, such as (i) the Redfield condition of extreme narrowing ($\Delta_s \tau_{RH} << 1$, Δ_s is the static ZFS), (ii) the ZFS energy should be much larger than the Zeeman energy ($E_{ZFS} >> E_{Zeeman}$), (iii) the electronic decay should be mono-exponential [24,25]. Outside these limits, a proper description of the electronic relaxation requires more complicated calculations that also take the static ZFS into account. Although the conditions for applying the SBM theory for the modeling of NMRD profiles are not always valid for Mn^{2+} complexes, this theory has been applied in almost all studies on the complexes mentioned in Table 1. It may be justified if the Redfield condition applies and if only data for *LF* > 10 MHz were considered [26], because then the influence of the electronic relaxation can be neglected. Otherwise, the SBM model can be applied for a qualitative description of structure relaxivity relationships when the best fit parameters obtained, particularly those concerning the electronic relaxation, are considered as effective rather than physically relevant [27]. The most relevant parameters governing the relaxivity as determined by fitting of NMRD profiles with the SBM equations are included in Table 1.
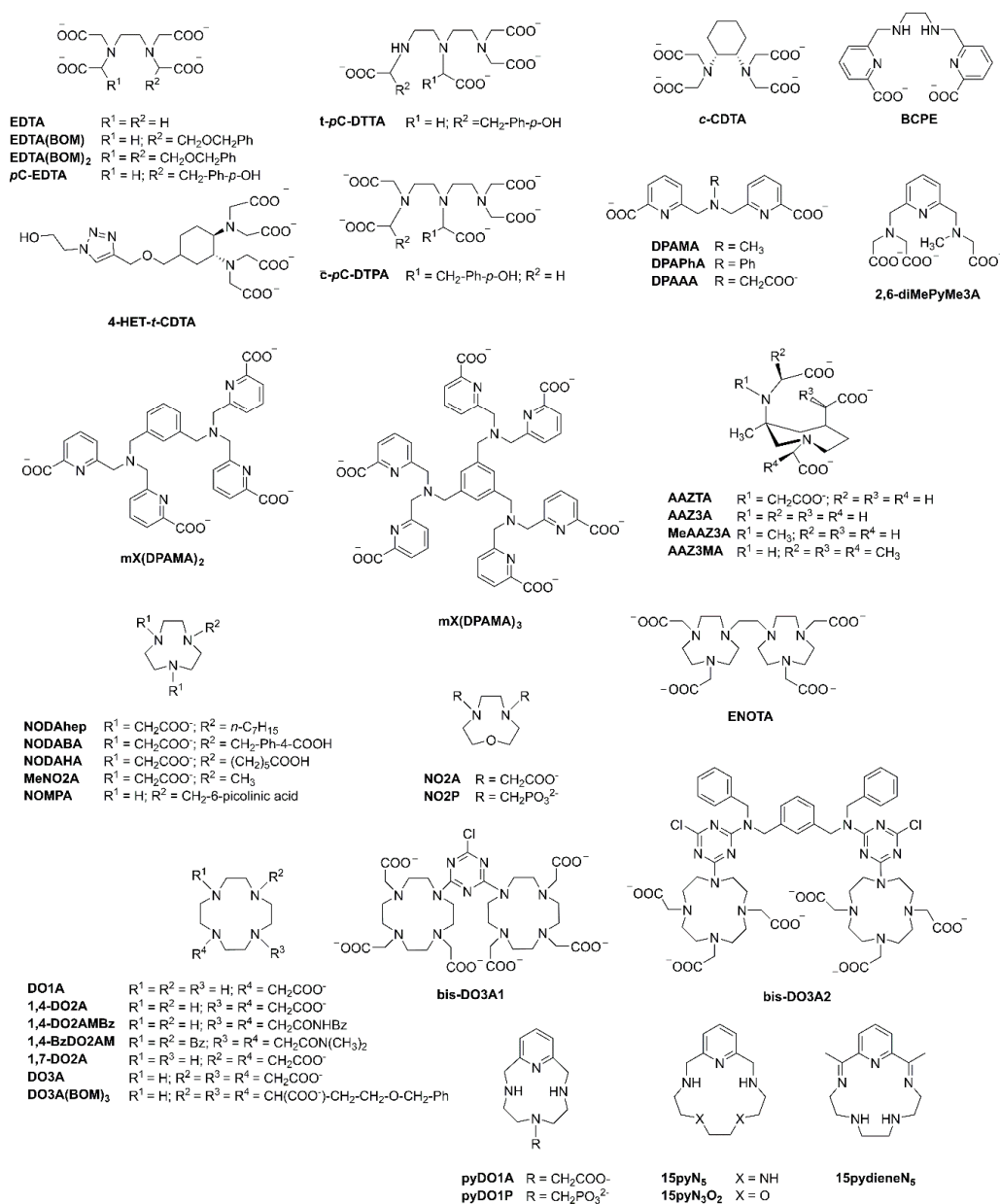

Figure 1. Structures of the organic ligands of the Mn^{2+} complexes mentioned in Table 1.

Table 1. Comparison of q_{lit} with q_{ref} as calculated with Equations (11) and (12) for the database of Mn^{2+} complexes. Other parameters of relevance for the relaxivity at 298 K and hyperfine coupling constants reported in the literature are included.

Organic Ligand	q_{lit} [a]	r_1 [b] $(s^{-1} \cdot mM^{-1})$	FW	q_{calc} [c]	τ_R [d] (ps)	τ_{S0} [d] (ps)	τ_M [d] (ns)	R_{MnH} [d] (Å)	$\lvert A_O/\hbar \rvert$ [d] $(10^6$ rad/s)	Ref.
DOTA	0.0	2.76	455.3	0.4	-	-	-	-	-	[28]
DTPA	0.0	2.40	390.2	0.4	-	-	-	-	-	[29]
DTPA	0.0	2.30	390.2	0.4	-	-	-	-	-	[30]
1,7-DO2A	0.0	2.53	341.3	0.4	-	152	-	-	-	[31]
NOTA	0.0	2.30	356.2	0.4	-	-	-	-	-	[28]
BCPE	0.0	2.23	383.3	0.4	-	87	-	-	-	[32]
DO3A	0.0	2.27	398.3	0.4	-	117	-	-	-	[31]
AAZTA	0.0	2.53	412.3	0.4	-	148	-	-	-	[33]
c-*p*C-DTPA	0.0	3.02	492.4	0.4	-	161	-	-	-	[34]
t-*p*C-DTTA	0.0	2.55	510.4	0.4	-	108	-	-	-	[34]
DO3A(BOM)$_3$	0.0	2.55	758.7	0.3	-	135	-	-	-	[35]
bis-DO3A1	0.0	2.27	837.8	0.3	-	93	-	-	-	[36]
bis-DO3A2	0.0	2.48	1340.3	0.3	-	137	-	-	-	[36]
AAZ3MA	0.2	3.04	415.3	0.5	51.0	96	7.52	2.81	8.7	[33]
MeAAZ3A	0.3	3.68	387.3	0.6	50.0	140	7.94	2.81	7.9	[33]
AAZ3A	0.6	5.05	373.3	0.8	50.0	158	21.3	2.81	7.2	[33]
1,4-DO2A	0.9	4.50	359.3	0.7	46.0	74	88.2	2.83	43.0	[31]
DO1A	1.0	4.04	302.3	0.7	22.0	88	0.168	2.83	39.4	[31]
MeNO2A	1.0	4.96	330.2	0.9	36.0	101	1.60	2.77	46.0	[37]
pyDO1A	1.0	3.54	336.3	0.6	23.0	449	0.330	-	-	[38]
NOMPA	1.0	6.21	336.3	1.1	51.2	129	0.361	2.77	−73.3	[39]
EDTA	1.0	5.41	361.2	0.9	56.0	81	2.12	2.83	40.5	[31]
EDTA	1.0	5.41	361.2	0.9	57.0	81	2.12	2.83	40.5	[31]
EDTA	1.0	5.81	361.2	1.0	-	-	-	-	-	[30]
EDTA	1.0	5.60	361.2	0.9	-	-	-	-	-	[29]
pyDO1P	1.0	3.84	371.2	0.6	38.6	36	0.565	-	39.9	[38]
NO2P	1.0	8.03	387.1	1.3	103.0	87	83.333	2.75	33.3	[40]
2,6-diMePyMe3A	1.0	5.23	395.2	0.8	46.0	52	0.357	2.83	26.4	[41]
NODAHep	1.0	8.10 [g]	414.4	1.3	84.0	37	370	2.75	30.0	[42]
DPAAA	1.0	6.75	415.2	1.0	47.6	146	7.94	2.76	31.5	[43]
c-CDTA	1.0	6.12	415.3	0.9	74.0	78	4.44	2.83	42.7	[44]
NODAHA	1.0	7.51 [g]	429.3	1.1	80.0	32	370	2.75	30.0	[42]
NODABA	1.0	9.80 [g]	449.3	1.5	121.0	37	769	2.75	30.0	[42]
t-*p*C-EDTA	1.0	5.93	467.3	0.9	75.4	80	-	2.92	-	[34]
EDTA(BOM)	1.0	5.61 [e]	495.3	0.8	83.7	87	10.7	2.90	-	[35]
1,4-DO2AMBz	1.0	5.67	539.6	0.8	85.0	71	5.71	2.83	33.0	[45]
4-HET-t-CDTA	1.0	6.72	570.4	0.9	104.9	56	5.68	2.83	40.0	[46]
1,4-BzDO2AM	1.0	5.89	595.7	0.8	96.0	60	3.95	2.83	31.0	[45]
EDTA(BOM)$_2$	1.0	7.25 [e]	629.5	0.9	110.8	84	7.60	2.90	-	[35]
ENOTA	1.0	6.46 [f]	658.5	0.8	85.0	4317	18.2	2.75	5.2	[23]
NO2A	1.4	5.67	317.2	1.0	22.0	160	0.840	2.75	33.3	[40]
15pyN$_5$	2.0	9.64	340.3	1.7	28.3	8710	14.5	2.81	38.6	[47]
15pyN$_3$O$_2$	2.0	11.52	342.3	2.0	40.3	7174	263	2.81	38.6	[47]
15pydieneN$_5$	2.0	14.20	364.3	2.3	-	-	-	-	-	[30]
DPAMA	2.0	11.25	390.3	1.8	47.8	167	3.27	2.74	-	[32]
DPAPhA	2.0	11.65	452.3	1.7	81.0	87	17.9	2.78	25.0	[43]
mX(DPAMA)$_2$	2.0	17.65	854.6	2.1	95.8	183	32.7	2.74	-	[32]
mX(DPAMA)$_3$	2.0	19.72	1243.8	2.2	136.0	173	32.7	2.74	-	[32]
none	6.0	19.52 [h]	163.0	5.6	30.0	26042	35.5	2.83	34.6	[13]
none	6.0	20.98 [i]	163.0	6.0	-	-	-	-	-	[30]

[a] As reported in reference. [b] Measured in reported NMRD profile at Larmor frequency (*LF*) = 0.01 MHz, unless stated otherwise. [c] As calculated with Equations (11) and (12). [d] Reported values evaluated from analysis of Nuclear Magnetic Relaxation Dispersion (NMRD) and ^{17}O NMRD data. [e] *LF* = 0.03 MHz. [f] *LF* =1.14 MHz. [g] *LF* = 0.02 MHz. [h] *LF* = 1.00 MHz. [i] *LF* = 1.35 MHz.

For the evaluation of *q*, we focused our attention to the low field parts of the NMRD profiles. Below the dispersion at *LF* ≈ 10 MHz, the profiles always had a plateau, where r_1 was rather large and almost independent of *LF*, which allows an accurate measurement of r_1. At low field, r_1 was dominated by *q* and the electronic relaxation, whereas at higher field strengths the nuclear relaxation dominated, which in turn was dominated by *q*, τ_R, and τ_M. This might lead to local maxima in the profile for high molecular weight compounds and relatively low relaxivities for low molecular compounds [2].

Values of r_1 at 0.01 MHz were measured in the profiles with a single dispersion. In the profiles for $[Mn(H_2O)_6]^{2+}$ and $[Mn_2(ENOTA)(H_2O)_2]$, the r_1 was measured at about 1 MHz (at the plateau behind the first dispersion), where the scalar contribution may be neglected.

Figure 2 displays a plot of the collected low field r_1-values versus the reported q values for the Mn^{2+} complexes concerned (q_{lit}). Many of the q_{lit} values were obtained by applying a combination of several of the methods described above. For $q = 0$, the datapoints are in a narrow range of r_1-values around an average of 2.4 ± 0.2 $s^{-1} \cdot mM^{-1}$. This value can therefore be applied as a good estimate of the outer sphere contribution of all Mn^{2+} complexes. For $q > 0$, Figure 2 clearly shows that the ranges of r_1 values for various q-values overlap. Hence r_1 ranges alone cannot be applied for the evaluation of q.
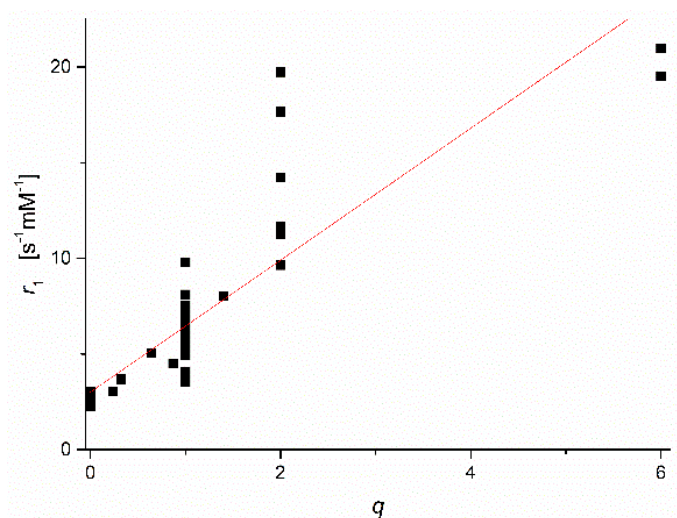

Figure 2. Plot of low field r_1 versus q-values collected from previously reported publications on Mn^{2+}-complexes.

A closer inspection of the structures corresponding with datapoints at $q = 1$ and $q = 2$ indicates that r_1 increased with the molecular volume of the Mn^{2+}-complexes at each q, which suggests that the r_1 at low field also depended on the rotational correlation time (τ_R). Therefore, we next considered the datapoints for $q \neq 0$. For these data, r_1/q appeared not to be linearly proportional to the molecular weight (FW). Regression of r_1/q as a function of FW with the computer program CurveExpert 1.4 using all in-built models afforded a good fit with Equation (11):

$$y = 9.16\left\{1 - exp\left(-2.97 \times FW \times 10^{-3}\right)\right\} \tag{11}$$

The hydration number can be calculated with Equation (12):

$$q_{calc} = \frac{r_1}{y} \tag{12}$$

Figure 3 shows the good agreement between the calculated hydration numbers (q_{calc}) and the values mentioned in the publications from which the r_1 values were taken (q_{lit}). Fractional q numbers are also correctly predicted. From Figure 3, the accuracy of q_{calc} is estimated to be ± 0.4. The good agreement between all calculated and reported q values indicates that the applied previously reported q values are correct. Moreover, it indicates that q and FW are the main parameters that determined the relaxivity; apparently, the influence of other parameters was rather small. This is surprising, since r_1 at low *LF* was expected to be dominated by the electronic relaxation. Even the q-values of complexes with relatively large τ_{S0}-values ($Mn_2(ENOTA)(H_2O)_2$, $[Mn(15pyN_5)(H_2O)]^{2+}$, $[Mn(15pyN_3O_2)(H_2O)_2]^{2+}$, and $[Mn(H_2O)_6]^{2+}$, see Table 1) seem to be predicted correctly. To explain this, simulations of r_1 at *LF*

= 0.01 MHz as a function of τ_M, τ_R, and τ_{S0} were made using the SBM equations. Figure 4 shows, for example, the simulations for typical $q = 1$ Mn^{2+} complexes. Figure 4A shows that r_1 is unsensitive to variations in τ_M; however, it is strongly dependent on τ_R, and Figure 4B shows that r_1 was only very sensitive to variations of τ_{S0} for complexes for which $\tau_R > 150$ ps. The complexes in the database used to deduce Equations (11) and (12) are exclusively of low and medium molecular weight compounds ($FW < 1250$). The simulations in Figure 4 confirmed that for those complexes, r_1 can be expected to be insensitive to variations in electronic relaxation rates and τ_M. However, it may be expected that these Equations are no longer valid for high molecular weight Mn^{2+} complexes. However, in those cases, q can generally be estimated from low molecular analogs.
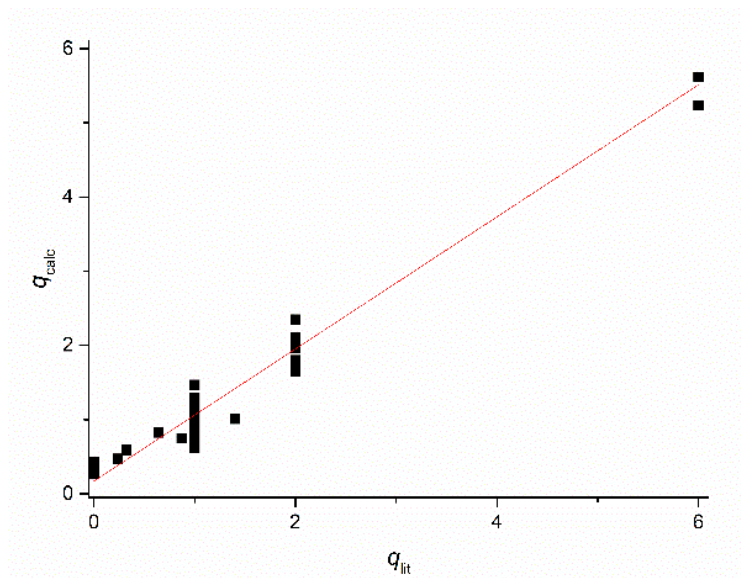

Figure 3. Plot of the hydration number for the Mn^{2+}-complexes mentioned in Table 1 calculated with Equations (1) and (2) (q_{calc}) versus the corresponding values reported in the literature (q_{lit}).
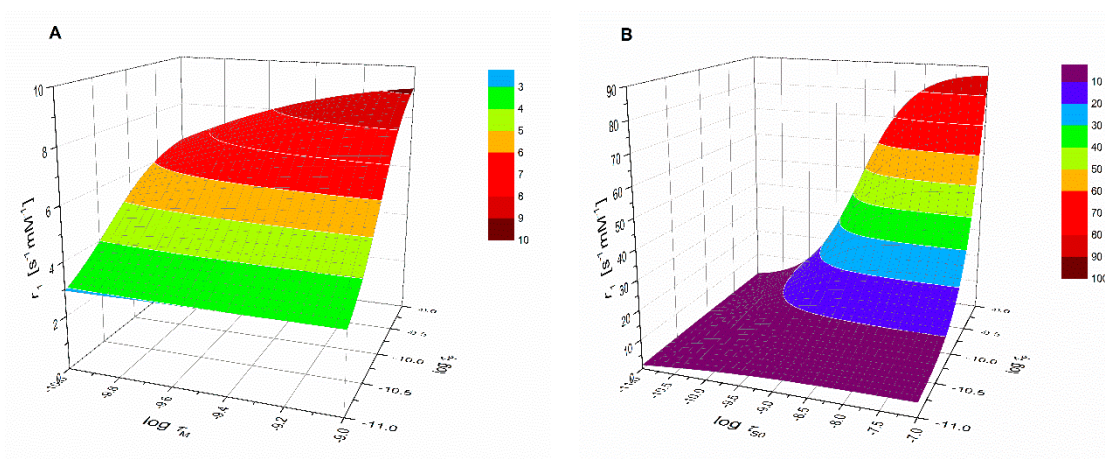

Figure 4. Representations of simulations of r_1 at $LF = 0.01$ MHz (**A**) as function of τ_M and τ_R and (**B**) as function of τ_{S0} and τ_R. Solomon-Bloembergen-Morgan (SBM) Equations (1)–(10) were applied using the following parameters: $q = 1$, $r_{MnH} = 2.83$ Å, $D_{MnH} = 2.31 \times 10^{-9}$ $m^2 \cdot s^{-1}$, $a_{MnH} = 3.6$ Å.

An attempt to apply a similar procedure for the evaluation of q from r_1 values at $LF = 60$ MHz resulted in unreasonable q_{calc} values that deviated substantially from q_{lit}.

3. Methods

The relaxivities were extracted from published NMRD profiles using the computer program WebPlotDigitizer, version 4.1 [48]. Equation (11) was selected with the computer program CurveExpert, version 1.4 [49].

4. Conclusions

An inspection of published ^{1}H NMRD profiles of Mn^{2+}-complexes of low and medium molecular weights ($FW < 1250$) shows that the magnitudes of r_1 at $LF \leq 0.1$ MHz is dominated by the parameters q and τ_R. Using a dataset of 49 published NMRD profiles as learning set, Equations (11) and (12) were evaluated for a quick and reliable estimation of q from r_1 values at $LF \leq 0.1$ MHz and the molecular weight of the complex.

References

1. Merbach, A.E.; Helm, L.; Tóth, É. *The Chemistry of Contrast Agents in Medical Magnetic Resonance Imaging*, 2nd ed.; John Wiley & Sons, Ltd.: Chichester, UK, 2013; ISBN 0-471-60778-9.

2. Caravan, P.; Ellison, J.J.; McMurry, T.J.; Lauffer, R.B. Gadolinium(III) chelates as MRI contrast agents: Structure, dynamics, and applications. *Chem. Rev.* **1999**, *99*, 2293–2352. [CrossRef] [PubMed]

3. Caravan, P.; Farrar, C.T.; Frullano, L.; Uppal, R. Influence of molecular parameters and increasing magnetic field strength on relaxivity of gadolinium- and manganese-based T_1 contrast agents. *Contrast Media Mol. Imaging* **2009**, *4*, 89–100. [CrossRef] [PubMed]

4. Baranyai, Z.; Brücher, E.; Uggeri, F.; Maiocchi, A.; Tóth, I.; Andrási, M.; Gáspár, A.; Zékány, L.; Aime, S. The role of equilibrium and kinetic properties in the dissociation of Gd[DTPA-bis(methylamide)] (omniscan) at near to physiological conditions. *Chem. Eur. J.* **2015**, *21*, 4789–4799. [CrossRef] [PubMed]

5. Brücher, E.; Tircsó, G.; Baranyai, Z.; Kovács, Z.; Sherry, A.D. Stability and toxicity of contrast agents. In *The Chemistry of Contrast Agents in Medical Magnetic Resonance Imaging*; Merbach, A.E., Helm, L., Tóth, É., Eds.; John Wiley & Sons Ltd.: Chichester, UK, 2013; pp. 157–208.

6. Kanal, E.; Tweedle, M.F. Residual or retained gadolinium: Practical implications for radiologists and our patients. *Radiology* **2015**, *275*, 630–634. [CrossRef] [PubMed]

7. Kanda, T.; Fukusato, T.; Matsuda, M.; Toyoda, K.; Oba, H.; Kotoku, J.I.; Haruyama, T.; Kitajima, K.; Furui, S. Gadolinium-based contrast agent accumulates in the brain even in subjects without severe renal dysfunction: Evaluation of autopsy brain specimens with inductively coupled plasma mass spectroscopy. *Radiology* **2015**, *276*, 228–232. [CrossRef] [PubMed]

8. Pullicino, R.; Radon, M.; Biswas, S.; Bhojak, M.; Das, K. A review of the current evidence on gadolinium deposition in the brain. *Clin. Neuroradiol.* **2018**, *128*, 159–169. [CrossRef] [PubMed]

9. Haynes, W.M. *CRC Handbook of Chemistry and Physics*; CRC Press: Boca Raton, FL, USA, 2014; ISBN 9781498754286.

10. Alpoim, M.C.; Urbano, A.M.; Geraldes, C.F.G.C.; Peters, J.A. Determination of the number of inner-sphere water-molecules in lanthanide(III) polyaminocarboxylate complexes. *J. Chem. Soc. Dalton Trans.* **1992**, 463–467. [CrossRef]

11. Djanashvili, K.; Peters, J.A. How to determine the number of inner-sphere water molecules in lanthanide(III) complexes by ^{17}O NMR spectroscopy. A technical note. *Contrast Media Mol. Imaging* **2007**, *2*, 67–71. [CrossRef] [PubMed]

12. Beeby, A.; Clarkson, I.M.; Dickins, R.S.; Faulkner, S.; Parker, D.; Royle, L.; de Sousa, A.S.; Williams, J.A.G.; Woods, M. Non-radiative deactivation of the excited states of europium, terbium and ytterbium complexes by proximate energy-matched OH, NH and CH oscillators: An improved luminescence method for establishing solution hydration states. *J. Chem. Soc. Perkin Trans.* **1999**, *2*, 493–504. [CrossRef]

13. Esteban-Gómez, D.; Cassino, C.; Botta, M.; Platas-Iglesias, C. ^{17}O and ^{1}H relaxometric and DFT study of hyperfine coupling constants in [Mn(H$_2$O)$_6$]$^{2+}$. *RSC Adv.* **2014**, *4*, 7094–7103. [CrossRef]

14. Póta, K.; Garda, Z.; Kálmán, F.K.; Barriada Pereira, J.L.; Esteban-Gómez, D.; Platas-Iglesias, C.; Tóth, I.; Brücher, E.; Tircsó, G. Making a next step toward inert Mn^{2+} complexes of open-chain ligands: The case of the rigid PhDTA ligand. *New J. Chem.* **2018**, *42*, 8001–8011. [CrossRef]

15. Leigh, J.S., Jr. Relaxation times in systems with chemical exchange. Exact solutions. *J. Magn. Reson.* **1971**, *4*, 308–311. [CrossRef]

16. Swift, T.J.; Connick, R.E. NMR (nuclear magnetic resonance)-relaxation mechanisms of O17 in aqueous solutions of paramagnetic cations and the lifetime of water molecules in the first coordination sphere. *J. Chem. Phys.* **1962**, *37*, 307–320. [CrossRef]

17. Solomon, I. Relaxation processes in a system of two spins. *Phys. Rev.* **1955**, *99*, 559–565. [CrossRef]

18. Bloembergen, N. Proton relaxation times in paramagnetic solutions. *J. Chem. Phys.* **1957**, *27*, 572–573. [CrossRef]

19. Bloembergen, N.; Morgan, L.O. Proton relaxation times in paramagnetic solutions. Effects of electron spin relaxation. *J. Chem. Phys.* **1961**, *34*, 842–850. [CrossRef]

20. Freed, J.H. Dynamic effects of pair correlation functions on spin relaxation by translational diffusion in liquids. II. Finite jumps and independent T$_1$ processes. *J. Chem. Phys.* **1978**, *68*, 4034–4037. [CrossRef]

21. Bertini, I.; Briganti, F.; Xia, Z.; Luchinat, C. Nuclear magnetic relaxation dispersion studies of hexaaquo manganese(II) ions in water-glycerol mixtures. *J. Magn. Reson.* **1993**, *101*, 198–201. [CrossRef]

22. Koenig, S.H.; Brown, R.D.; Studebaker, J. On the interpretation of solvent proton magnetic relaxation data with particular application to the structure of the active site of Mn-carboxypeptidase A. In *Cold Spring Harbor Symposia on Quantitative Biology*; Cold Spring Harbor Laboratory Press: Cold Spring Harbor, New York, NY, USA, 1971; Volume 36, pp. 551–559.

23. Balogh, E.; He, Z.; Hsieh, W.; Liu, S.; Tóth, É. Dinuclear complexes formed with the triazacyclononane derivative ENOTA^{4-}: High-pressure ^{17}O NMR evidence of an associative water exchange on [Mn^{II}$_2$(ENOTA)(H$_2$O)$_2$]. *Inorg. Chem.* **2007**, *46*, 238–250. [CrossRef] [PubMed]

24. Helm, L. Relaxivity in paramagnetic systems: Theory and mechanism. *Prog. Nucl. Magn. Reson. Spectrosc.* **2006**, *49*, 45–64. [CrossRef]

25. Belorizky, E.; Fries, P.H.; Helm, L.; Kowalewski, J.; Kruk, D.; Sharp, R.R.; Westlund, P.O. Comparison of different methods for calculating the paramagnetic relaxation enhancement of nuclear spins as a function of the magnetic field. *J. Chem. Phys.* **2008**, *128*, 052315. [CrossRef] [PubMed]

26. Troughton, J.S.; Greenfield, M.T.; Greenwood, J.M.; Dumas, S.; Wiethoff, A.J.; Wang, J.; Spiller, M.; McMurry, T.J.; Caravan, P. Synthesis and evaluation of a high relaxivity manganese(II)-based MRI contrast agent. *Inorg. Chem.* **2004**, *43*, 6313–6323. [CrossRef] [PubMed]

27. Belorizky, E.; Fries, P.H. Simple analytical approximation of the longitudinal electronic relaxation rate of Gd(III) complexes in solutions. *Phys. Chem. Chem. Phys.* **2004**, *6*, 2341–2351. [CrossRef]

28. Geraldes, C.F.G.C.; Sherry, A.D.; Brown, R.D., III; Koenig, S.H. Magnetic field dependence of solvent proton relaxation rates induced by gadolinium(3+) and manganese(2+) complexes of various polyaza macrocyclic ligands: Implications for NMR imaging. *Magn. Reson. Med.* **1986**, *3*, 242–250. [CrossRef] [PubMed]

29. Koenig, S.H.; Brown, R.D., III. Relaxometry of magnetic resonance imaging contrast agents. *Magn. Reson. Annu.* **1987**, 263–286.

30. Jackels, S.C.; Durham, M.M.; Newton, J.E.; Henninger, T.C. Aqueous proton NMR relaxation enhancement by manganese(II) macrocyclic complexes: Structure-relaxivity relationships. *Inorg. Chem.* **1992**, *31*, 234–239. [CrossRef]

31. Rolla, G.A.; Platas-Iglesias, C.; Botta, M.; Tei, L.; Helm, L. ^{1}H and ^{17}O NMR relaxometric and computational study on macrocyclic Mn(II) complexes. *Inorg. Chem.* **2013**, *52*, 3268–3279. [CrossRef] [PubMed]

32. Forgács, A.; Botta, M.; Regueiro-Figueroa, M.; Barriada, J.L.; Esteban-Gómez, D.; de Blas, A.; Rodríguez-Blas, T.; Platas-Iglesias, C. Mono-, bi-, and trinuclear bis-hydrated Mn(2+) complexes as potential MRI contrast agents. *Inorg. Chem.* **2015**, *54*, 9576–9587. [CrossRef] [PubMed]

33. Tei, L.; Gugliotta, G.; Fekete, M.; Kalman, F.K.; Botta, M. Mn(II) complexes of novel hexadentate AAZTA-like chelators: A solution thermodynamics and relaxometric study. *Dalton Trans.* **2011**, *40*, 2025–2032. [CrossRef] [PubMed]

34. Rolla, G.A.; Tei, L.; Fekete, M.; Arena, F.; Gianolio, E.; Botta, M. Responsive Mn(II) complexes for potential applications in diagnostic magnetic resonance imaging. *Bioorg. Med. Chem.* **2011**, *19*, 1115–1122. [CrossRef] [PubMed]

35. Aime, S.; Anelli, L.; Botta, M.; Brocchetta, M.; Canton, S.; Fedeli, F.; Gianolio, E.; Terreno, E. Relaxometric evaluation of novel manganese(II) complexes for application as contrast agents in magnetic resonance imaging. *J. Biol. Inorg. Chem.* **2002**, *7*, 58–67. [CrossRef] [PubMed]

36. Artali, R.; Baranyai, Z.; Botta, M.; Giovenzana, G.B.; Maspero, A.; Negri, R.; Palmisano, G.; Sisti, M.; Tollari, S. Solution thermodynamics, computational and relaxometric studies of ditopic DO3A-based Mn(II) complexes. *New J. Chem.* **2015**, *39*, 539–547. [CrossRef]

37. Patinec, V.; Rolla, G.A.; Botta, M.; Tripier, R.; Esteban-Gómez, D.; Platas-Iglesias, C. Hyperfine coupling constants on inner-sphere water molecules of a triazacyclononane-based Mn(II) complex and related systems relevant as mri contrast agents. *Inorg. Chem.* **2013**, *52*, 11173–11184. [CrossRef] [PubMed]

38. Drahoš, B.; Kotek, J.; Císařová, I.; Hermann, P.; Helm, L.; Lukeš, I.; Tóth, É. Mn^{2+} complexes with 12-membered pyridine based macrocycles bearing carboxylate or phosphonate pendant arm: Crystallographic, thermodynamic, kinetic, redox, and $^1H/^{17}O$ relaxation studies. *Inorg. Chem.* **2011**, *50*, 12785–12801. [CrossRef] [PubMed]

39. Molnár, E.; Camus, N.; Patinec, V.; Rolla, G.A.; Botta, M.; Tircsó, G.; Kálmán, F.K.; Fodor, T.; Tripier, R.; Platas-Iglesias, C. Picolinate-containing macrocyclic Mn^{2+} complexes as potential MRI contrast agents. *Inorg. Chem.* **2014**, *53*, 5136–5149. [CrossRef] [PubMed]

40. Drahoš, B.; Pniok, M.; Havlíčková, J.; Kotek, J.; Císařová, I.; Hermann, P.; Lukeš, I.; Tóth, É. Mn^{2+} complexes of 1-oxa-4,7-diazacyclononane based ligands with acetic, phosphonic and phosphinic acid pendant arms: Stability and relaxation studies. *Dalton Trans.* **2011**, *40*, 10131–10146. [CrossRef] [PubMed]

41. Laine, S.; Bonnet, C.S.; Kálmán, F.K.; Garda, Z.; Pallier, A.; Caillé, F.; Suzenet, F.; Tircsó, G.; Tóth, É. Mn^{2+} complexes of open-chain ligands with a pyridine backbone: Less donor atoms lead to higher kinetic inertness. *New J. Chem.* **2018**, *42*, 8012–8020. [CrossRef]

42. De Sá, A.; Bonnet, C.S.; Geraldes, C.F.G.C.; Tóth, É.; Ferreira, P.M.T.; André, J.P. Thermodynamic stability and relaxation studies of small, triaza-macrocyclic Mn(II) chelates. *Dalton Trans.* **2013**, *42*, 4522–4532. [CrossRef] [PubMed]

43. Forgács, A.; Pujales-Paradela, R.; Regueiro-Figueroa, M.; Valencia, L.; Esteban-Gómez, D.; Botta, M.; Platas-Iglesias, C. Developing the family of picolinate ligands for Mn^{2+} complexation. *Dalton Trans.* **2017**, 1546–1558. [CrossRef] [PubMed]

44. Molnár, E.; Váradi, B.; Garda, Z.; Botár, R.; Kálmán, F.K.; Tóth, É.; Platas-Iglesias, C.; Tóth, I.; Brücher, E.; Tircsó, G. Remarkable differences and similarities between the isomeric Mn(II)-*cis-* and *trans*-1,2-diaminocyclohexane-*N,N,N′,N′*-tetraacetate complexes. *Inorg. Chim. Acta* **2018**, *472*, 254–263. [CrossRef]

45. Forgács, A.; Tei, L.; Baranyai, Z.; Esteban-Gómez, D.; Platas-Iglesias, C.; Botta, M. Optimising the relaxivities of Mn^{2+} complexes by targeting human serum albumin (HSA). *Dalton Trans.* **2017**, 8494–8504. [CrossRef] [PubMed]

46. Vanasschen, C.; Molnár, E.; Tircsó, G.; Kálmán, F.K.; Tóth, É.; Brandt, M.; Coenen, H.H.; Neumaier, B. Novel cdta-based, bifunctional chelators for stable and inert Mn^{II} complexation: Synthesis and physicochemical characterization. *Inorg. Chem.* **2017**, *56*, 7746–7760. [CrossRef] [PubMed]

47. Drahoš, B.; Kotek, J.; Hermann, P.; Lukeš, I.; Tóth, É. Mn^{2+} complexes with pyridine-containing 15-membered macrocycles: Thermodynamic, kinetic, crystallographic, and $^1H/^{17}O$ relaxation studies. *Inorg. Chem.* **2010**, *49*, 3224–3238. [CrossRef] [PubMed]

48. Webplotdigitizer. Available online: https://automeris.io/WebPlotDigitizer/ (accessed on 10 August 2018).

49. Curveexpert Basic, Version 2.1.0. Available online: http://www.curveexpert.net (accessed on 10 August 2018).